Acoustic response of a rigid-frame porous medium plate with a periodic set of inclusions

J.-P. Groby[a)]
CMAP, CNRS/École Polytechnique, UMR7641, F-91128 Palaiseau Cedex, France

A. Wirgin[b)]
Laboratoire de Mécanique et d'Acoustique, CNRS, UPR7051, Marseille, France

L. De Ryck[c)] and W. Lauriks
Laboratory of Acoustics and Thermal Physics, KULeuven, Heverlee, Belgium

R. P. Gilbert
Department of Mathematical Sciences, University of Delaware, Newark, Delaware 19716

Y. S. Xu
Department of Mathematics, University of Louisville, Louisville, Kentucky 40292

(Received 2 March 2009; revised 2 June 2009; accepted 2 June 2009)

The acoustic response of a rigid-frame porous plate with a periodic set of inclusions is investigated by a multipole method. The acoustic properties, in particular, the absorption, of such a structure are then derived and studied. Numerical results together with a modal analysis show that the addition of a periodic set of high-contrast inclusions leads to the excitation of the modes of the plate and to a large increase in the acoustic absorption. © *2009 Acoustical Society of America.*
[DOI: 10.1121/1.3158936]

PACS number(s): 43.55.Ev, 43.20.Fn, 43.20.Ks, 43.20.Gp [NX] Pages: 685–693

I. INTRODUCTION

This work was initially motivated by the design problem connected with the determination of the optimal profile of a continuous and/or discontinuous spatial distribution of the material/geometric properties of porous materials for the absorption of sound. Porous materials (foam) suffer from a lack of absorption particularly at low frequency, when compared to its value at higher frequency, and for normal incidence. The usual way to solve this problem is by multi-layering.[1–3] The purpose of the present article is to investigate an alternative to multi-layering by embedding a periodic set of inclusions, whose size is not small compared with the wavelength, in an otherwise macroscopically-homogeneous porous plate whose thickness and weight are relatively small (i.e., the principal constraints in the design of acoustic absorbing materials).

Acoustic wave propagation in porous materials was mainly studied in order to deal with sound absorption, material property characterization, etc. Homogeneous porous materials are well described by the first work of Biot[4,5] and later contributions.[6–8] On the other hand, the equation that describes acoustic wave propagation in a macroscopically-inhomogeneous rigid-frame porous medium was only recently derived in Ref. 9 from the alternative formulation of Biot's theory.[5] The latter equation could eventually offer an alternative to multi-layering in the sense that it can be applied to the design of (e.g., functionally gradient) rigid-frame media with continuously-varying properties.

The influence of the addition of a volumic heterogeneity on absorption and transmission of porous plates was previously studied by means of the homogenization procedure. In Ref. 10, the authors considered the reflection of a plane acoustic wave by a porous plate that presents a periodic set of pits oriented along the direction of propagation. The medium is homogenized, generalized expressions for the complex bulk modulus and dynamic permeability of double-porosity media are presented, and its behavior is described in Ref. 11. This leads to a drastic increase in the absorption coefficient at low frequency. In Ref. 12, the authors considered the transmission of an acoustic wave through a porous medium in which a set of randomly-arranged metallic rods is embedded. This medium is converted, by a procedure called *ISA*β, into an equivalent homogeneous medium, which exhibits decreased transmission and increased absorption. Herein, the diffraction of a plane wave by a porous plate in which is embedded a periodic set of porous or high-contrast (Neumann type condition) inclusions is studied with the help of the so-called multipole-method.[13–15] The field scattered by the inclusions is fully accounted-for so that a complete description of the effects, in terms of increase in the absorption, is made possible.

Periodic arrangements of either surface irregularities or volume heterogeneities usually lead to energy entrapment either at the surface or inside the structure, this being strongly linked to mode excitation and to an increase in the absorption coefficient (first noticed by Wood[16] and partially ex-

[a)]Electronic mail: jeanphilippe.groby@fys.kuleuven.be
[b)]Present address: Laboratory of Acoustics and Thermal Physics, Celestijnenlaan 200D, B-3001 Leuven, Belgium.
[c)]Present address: LMS International NV, 3001 Leuven, Belgium.

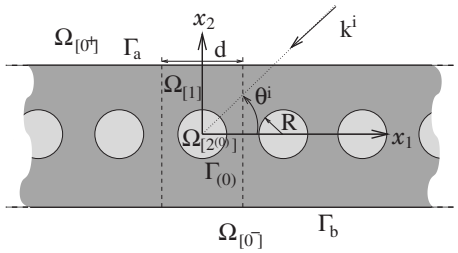

FIG. 1. Sagittal plane representation of the configuration of plane wave solicitation of a d-periodic porous fluid-like plate with fluid-like inclusions (of radius R).

plained by Cutler[17]). The particular properties of such structures have been studied in mechanics, with application to composite materials,[18–20] in optics initially motivated by the collection of solar energy[21,22] with applications to photonic crystals,[23,24] in electromagnetics with application to so-called left-handed materials,[25] and in geophysics for the study of the "city-site" effect.[26,27] The properties of such structures are now studied to create band-gaps for elastic or acoustic waves (phononic/sonic crystals[28–30]), and have been used for the design of sound absorbing or porous materials.[31–34]

II. FORMULATION OF THE PROBLEM

A. Description of the configuration

Both the incident plane acoustic wave and the plate are assumed to be invariant with respect to the Cartesian coordinate x_3. A sagittal x_1-x_2 plane view of the two-dimensional scattering problem is given in Fig. 1.

Before the introduction of the cylindrical inclusions, the plate is made of a porous material (e.g., a foam) which is modeled (by homogenization) as a (macroscopically-homogeneous) equivalent fluid $M^{[1]}$. Another equivalent fluid medium $M^{[2]}$ occupies each cylindrical inclusion. In the sagittal plane, the jth cylinder is the circular disk $\Omega_{[2^{(j)}]}$. Two subspaces $\Omega_{[1^\pm]}$ are also created, respectively, corresponding to the upper and lower parts of the plate containing the inclusions. The host medium $M^{[0]}$ occupying the two half spaces $\Omega_{[0^\pm]}$ is air. Thus, the plate is macroscopically-inhomogeneous, the heterogeneity being periodic in the x_1 direction with period d.

The upper and lower flat, mutually-parallel boundaries of the plate are Γ_a and Γ_b in the sagittal plane. The x_2 coordinates of these lines are a and b, the thickness L of the plate being $L=a-b$. The circular boundary of $\Omega_{[2^{(j)}]}$ is $\Gamma_{(j)}$. The center of the $j=0$ disk is at the origin O of the laboratory system $Ox_1x_2x_3$. The union of $\Omega_{[0^+]}$ and $\Omega_{[0^-]}$ is denoted by $\Omega_{[0]}$.

The wavevector $\mathbf{k}^i$ of the incident plane wave lies in the sagittal plane and the angle of incidence is θ^i measured counterclockwise from the positive x_1 axis.

B. Wave equations

Total pressure, wavenumber, and wave speed are designated by the generic symbols p, k, and c respectively, with $p=p^{[j]}$, $k=k^{[j]}=\omega/c^{[j]}$ in $\Omega_{[j]}$, $j=0^\pm,1,2^{(j)}$.

Rather than solve directly for the pressure $p(\mathbf{x},t)$ [with $\mathbf{x}=(x_1,x_2)$], $\tilde{p}(\mathbf{x},\omega)$ is preferred, related to $p(\mathbf{x},t)$ by the Fourier transform $p(\mathbf{x},t)=\int_{-\infty}^{\infty}\tilde{p}(\mathbf{x},\omega)e^{-i\omega t}d\omega$. Henceforth, the ω is dropped in $\tilde{p}(\mathbf{x},\omega)$ so as to designate the latter by $\tilde{p}(\mathbf{x})$.

The effective compressibility and density of medium $M^{[1]}$, linked to the sound speed through $c^{[1]}=\sqrt{1/(K^{[1]}\rho^{[1]})}$, are[8,9]

$$\frac{1}{K^{[1]}}=\frac{\gamma P_0}{\phi\left(\gamma-(\gamma-1)\left(1+i\frac{\omega_c}{\mathrm{Pr}\omega}G(\mathrm{Pr}\omega)\right)^{-1}\right)},$$

$$\rho^{[1]}=\frac{\rho_f\alpha_\infty}{\phi}\left(1+i\frac{\omega_c}{\omega}F(\omega)\right), \tag{1}$$

wherein $\omega_c=\sigma\phi/\rho_f\alpha_\infty$ is the Biot characteristic frequency, γ is the specific heat ratio, P_0 is the atmospheric pressure, Pr is the Prandtl number, ρ_f is the density of the fluid in the (interconnected) pores, ϕ is the porosity, α_∞ is the tortuosity, and σ is the flow resistivity. The correction functions $G(\mathrm{Pr}\omega)$ (Ref. 35) and $F(\omega)$ (Ref. 6) are given by

$$G(\mathrm{Pr}\omega)=\sqrt{1-4i\frac{\eta\rho_f\alpha_\infty^2}{\sigma^2\phi^2\Lambda'^2}\mathrm{Pr}\omega},$$

$$F(\omega)=\sqrt{1-4i\frac{\eta\rho_f\alpha_\infty^2}{\sigma^2\phi^2\Lambda^2}\omega}, \tag{2}$$

wherein η is the viscosity of the fluid, Λ' is the thermal characteristic length, and Λ is the viscous characteristic length.

The incident wave propagates in $\Omega_{[0^+]}$ and is expressed by $\tilde{p}^i(\mathbf{x})=A^ie^{i(k_1^ix_1-k_2^i(x_2-a))}$, wherein $k_1^i=-k^{[0]}\cos\theta^i$, $k_2^i=k^{[0]}\sin\theta^i$, and $A^i=A^i(\omega)$ is the signal spectrum.

The particular feature of the problem is the transverse periodicity of $\cup_{j\in\mathbb{Z}}\Omega_{[2^{(j)}]}$. The plane wave nature of the incident wave and the periodic nature of $\cup_{j\in\mathbb{Z}}\Omega_{[2^{(j)}]}$ imply the Floquet relation

$$\tilde{p}(x_1+nd,x_2)=\tilde{p}(x_1,x_2)e^{ik_1^ind},\quad \forall n\in\mathbb{Z}. \tag{3}$$

Consequently, it suffices to determine the field in the central cell of the plate which includes the disk $\Omega_{[2^{(0)}]}$ in order to obtain the fields, via the Floquet relation, in the other cells. Henceforth, the simplified notation is adopted: $\Omega_{[2]}:=\Omega_{[2^{(0)}]}$, $\Gamma:=\Gamma_{[(0)]}$, and $\tilde{p}^{[2]}=\tilde{p}^{[2^{(0)}]}$.

C. Boundary and radiation conditions

Since $M^{[0]}$ and $M^{[1]}$ are fluid-like, the pressure and the normal velocity are continuous across the interfaces Γ_a and Γ_b:

$$\tilde{p}^{[0^+]}(\mathbf{x})-\tilde{p}^{[1]}(\mathbf{x})=0,\quad \forall\mathbf{x}\in\Gamma_a,$$

$$\partial_n\tilde{p}^{[0^+]}(\mathbf{x})/\rho^{[0]}-\partial_n\tilde{p}^{[1]}(\mathbf{x})/\rho^{[1]}=0,\quad \forall\mathbf{x}\in\Gamma_a,$$

$$\tilde{p}^{[0^-]}(\mathbf{x})-\tilde{p}^{[1]}(\mathbf{x})=0,\quad \forall\mathbf{x}\in\Gamma_b,$$

$$\partial_n \tilde{p}^{[0^-]}(\mathbf{x})/\rho^{[0]} - \partial_n \tilde{p}^{[1]}(\mathbf{x})/\rho^{[0]} = 0, \quad \forall\, \mathbf{x} \in \Gamma_b, \tag{4}$$

wherein $\mathbf{n}$ denotes the generic unit vector normal to a boundary and ∂_n designates the operator $\partial_n = \mathbf{n}\cdot\nabla$.

Since $M^{[1]}$ and $M^{[2]}$ are fluid-like, the pressure and normal velocity are continuous across the interface Γ:

$$\tilde{p}^{[2]}(\mathbf{x}) - \tilde{p}^{[1]}(\mathbf{x}) = 0, \quad \forall\, \mathbf{x} \in \Gamma,$$

$$\partial_n \tilde{p}^{[2]}(\mathbf{x})/\rho^{[2]} - \partial_n \tilde{p}^{[1]}(\mathbf{x})/\rho^{[1]} = 0, \quad \forall\, \mathbf{x} \in \Gamma. \tag{5}$$

When the contrast between the media $M^{[1]}$ and $M^{[2]}$ is high, i.e., high-contrast inclusions, the latter can be approximated as infinitely rigid. In this case, the boundary conditions across the interface Γ no longer depend on the fields inside the inclusions, i.e., on the internal geometry of $\Omega_{[2]}$ and on the material characteristics of $M^{[2]}$ (except its rigid behavior), and reduce to Neumann type boundary conditions:

$$\partial_n \tilde{p}^{[1]}(\mathbf{x}) = 0, \quad \forall\, \mathbf{x} \in \Gamma. \tag{6}$$

The uniqueness of the solution to the forward-scattering problem is assured by the radiation conditions:

$$\tilde{p}^{[0^+]}(\mathbf{x}) - \tilde{p}^{i}(\mathbf{x}) \sim \text{outgoing waves}, \quad \forall\, \mathbf{x} \to \infty,$$

$$\tilde{p}^{[0^-]}(\mathbf{x}) \sim \text{outgoing waves}, \quad \forall\, \mathbf{x} \to \infty. \tag{7}$$

III. FIELD REPRESENTATIONS IN $\Omega_{[0^\pm]}$, $\Omega_{[2]}$, AND $\Omega_{[1^\pm]}$

Separation of variables, the radiation conditions, and the Floquet relation lead to the following representations:

$$\tilde{p}^{[0^+]}(\mathbf{x}) = \sum_{p\in\mathbb{Z}} [A^i e^{-ik_{2p}^{[0]}(x_2-a)}\delta_{p0} + R_p e^{ik_{2p}^{[0]}(x_2-a)}]e^{ik_{1p}x_1}, \tag{8}$$

$$\tilde{p}^{[0^-]}(\mathbf{x}) = \sum_{p\in\mathbb{Z}} T_p e^{i(k_{1p}x_1 - k_{2p}^{[0]}(x_2-b))}, \tag{9}$$

wherein R_p and T_p are, respectively, the reflection and transmission coefficients of the plane wave indiced by p, δ_{p0} the Kronecker symbol, $k_{1p} = k_1^i + 2p\pi/d$, and $k_{2p}^{[0]} = \sqrt{(k^{[0]})^2 - (k_{1p})^2}$, with $\mathrm{Re}(k_{2p}^{[0]}) \geq 0$ and $\mathrm{Im}(k_{2p}^{[0]}) \geq 0$ for $\omega \geq 0$.

The field in the central inclusion, with $[\mathbf{r} = (r,\theta)]$, takes the form

$$\tilde{p}^{[2]}(\mathbf{r}) = \sum_{l\in\mathbb{Z}} C_l J_l(k^{[2]} r) e^{il\theta}, \tag{10}$$

wherein J_l is the lth order Bessel function and C_l are the coefficients of the field scattered inside the cylinder of the unit cell.

It is convenient to use Cartesian coordinates (x_1, x_2) to write the field representation in $\Omega_{[1^\pm]}$. The latter takes the form of the sum (by use of the superposition principle) of the field diffracted by the inclusions and the diffracted field in the plate.[34] Because of the periodic nature of the configuration, the diffracted field in the plate can be written in Cartesian coordinates as

$$\tilde{p}^{[1^\pm]}(\mathbf{x}) = \sum_{p\in\mathbb{Z}} (f_p^{[1]-} e^{-ik_{2p}^{[1]}x_2} + f_p^{[1]+} e^{ik_{2p}^{[1]}x_2}) e^{ik_{1p}x_1} + \sum_{p\in\mathbb{Z}} \sum_{l\in\mathbb{Z}} B_l K_{pl}^{\pm} e^{i(k_{1p}x_1 \pm k_{2p}^{[1]}x_2)}, \tag{11}$$

where $f_p^{[1^\pm]}$ accounts for the diffracted field by the plate, B_l are the coefficients of the field scattered by the cylinder of the unit cell, the signs + and − correspond to $x_2 > R$ and $x_2 < (-R)$, respectively, and $K_{pm}^{\pm} = 2(-i)^m e^{\pm im\theta_p}/dk_{2p}^1$, with θ_p such that $k^{[1]}e^{i\theta_p} = k_{1p} + ik_{2p}^{[1]}$.[13,15]

IV. THE REFLECTED AND TRANSMITTED FIELDS

The method of resolution of the problem is described in Appendix A. Once Eq. (A7) is solved for B_l, $\forall l \in \mathbb{Z}$, expressions for R_p and T_p depending on B_l, $\forall l \in \mathbb{Z}$, are derived from the linear system (A1):

$$R_P = \frac{2A^i i \sin(k_2^{[1]i}L)((\alpha^{[0]i})^2 - (\alpha^{[1]i})^2)}{D_0^i} + \sum_{p\in\mathbb{Z}}\sum_{l\in\mathbb{Z}} \frac{8(-i^l)B_l}{dk_{2p}^{[1]}} \times \frac{\alpha_p^{[1]}(-i\alpha_p^{[0]}\sin(l\theta_p + k_{2p}^{[1]}b) - \alpha_p^{[1]}\cos(l\theta_p + k_{2p}^{[1]}b))}{D_p},$$

$$T_P = \frac{-A^i 4\alpha^{[1]i}\alpha^{[0]i}}{D_0^i} + \sum_{p\in\mathbb{Z}}\sum_{l\in\mathbb{Z}} \frac{8(-i^l)B_l}{dk_{2p}^{[1]}} \times \frac{\alpha_p^{[1]}(i\alpha_p^{[0]}\sin(l\theta_p + k_{2p}^{[1]}a) - \alpha_p^{[1]}\cos(l\theta_p + k_{2p}^{[1]}a))}{D_p}, \tag{12}$$

with

$$D_p = 2i\sin(k_{2p}^{[1]}L)((\alpha_p^{[0]})^2 + (\alpha_p^{[1]})^2) - 4\alpha_p^{[0]}\alpha_p^{[1]}\cos(k_{2p}^{[1]}L), \tag{13}$$

and $D_0^i = D_0$. Introducing the latter equation into Eqs. (8) and (9) leads to the expression of the pressure field in $\Omega_{[0^\pm]}$. In particular, the latter fields (and also in $\Omega_{[1]}$), are the sum of (i) the field in absence of the inclusions (whose expressions are the same as those in Ref. 36) and (ii) the field due to the presence of the inclusions. The latter field, when compared with the Green's function as calculated in Ref. 36 in the case of a line source located in the plate without inclusions, takes the form of the field radiated by induced periodic sources located on Γ. The latter do not add energy to the system, but rather entail a redistribution of the energy in the frequency range of the solicitation and allow the presence of evanescent waves in the ambient media whereby it is possible to excite modes.

Both the method of resolution (including the numerical recipes, Appendix B) and field expression were validated with the help of the authors' finite-element code[37] in the case of a dissipative plate in which a number of dissipative inclusions are embedded, large enough for the situation in the central part of the configuration to be very close to that described by the multipole method in the case of an infinite number of inclusions.

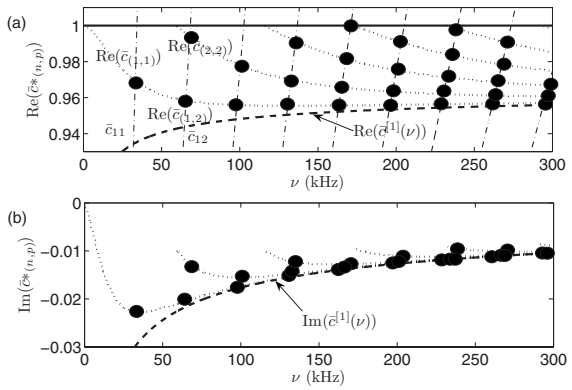

FIG. 2. (a) Real part and (b) imaginary part of the roots of the dispersion relation of a $L=10\times10^{-3}$ m thick porous plate: $(\cdots)\bar{c}^\star(\nu)$, (—) $\bar{c}^{[0]}$, and (- - -) $\bar{c}^{[1]}(\nu)$. Modified modes of the plate and the associated attenuation for period $d=10\times10^{-3}$ m are pointed out by a dot.

V. MODAL ANALYSIS

A. Modal analysis in the absence of inclusions

In the absence of inclusions, the coefficients of the field scattered by the inclusions vanish ($B_l=0,\ \forall l\in\mathbb{Z}$) and all the unknowns that are indexed by p reduce to their value for $p=0$. The problem reduces to the determination of $R=R_p\delta_{p0}$, $T=T_p\delta_{p0}$, $f^{[1]-}=f_p^{[1]-}\delta_{p0}$, and $f^{[1]+}=f_p^{[1]+}\delta_{p0}$ from the corresponding linear system (A1).

The natural modes of the configuration are obtained by turning off the excitation (i.e., $A^i=0$). The resulting matrix equation possesses a non-trivial solution only if the determinant of the matrix vanishes, i.e.,

$$D_0^i = 2i((\alpha^{[0]i})^2+(\alpha^{[1]i})^2)\sin(k_2^{[1]i}L) - 4\alpha^{[1]i}\alpha^{[0]i}\cos(k_2^{[1]i}L)=0, \tag{14}$$

whose roots take the form of a couple $(k_1^\star,\omega)$, defining the wavenumbers and natural frequencies of the modes of the configuration. For a non-dissipative medium in the plate, $k_1^\star$ and ω are both real. In the case of interest here, the medium filling the plate is dissipative so that $k_1^\star$ is complex. Each mode of the configuration occurs at a wavenumber corresponding to the real part of $k_1^\star$, to which an attenuation corresponding to the imaginary part of $k_1^\star$ is associated.

Figure 2 depicts the real and the imaginary parts of the solution $c^\star(\omega)=\omega/(k_1^\star)$ of Eq. (14) with the mechanical and geometrical characteristics used in Sec. VII A. The solution is normalized by $c^{[0]}$ defining $\bar{c}^\star(\omega)=c^\star(\omega)/c^{[0]}$. The procedure used to solve the dispersion relation latter is based on the one already employed in Ref. 38. For a fixed frequency, the dispersion relation can have more than one root $\bar{c}^\star(\omega)$. They are identified in the following by $\bar{c}^\star_{(n)}(\omega)$, $n\in\mathbb{N}$. An important remark is that the dispersion relation cannot vanish when the incident wave takes the form of a plane wave because $\mathrm{Re}(k_1^\star)\geq k^{[0]}$ for Eq. (14) to be true, whereas $k_1^i\in[-k^{[0]},k^{[0]}]$ in the case of an incident plane (bulk) wave. In the absence of the inclusions, no modes of the configuration can be excited when a plane (bulk) wave strikes the plate.

B. Modal analysis with inclusions

For the plate with periodic inclusions, the problem reduces to the resolution of the linear system (A7). As previously, the natural modes of the configuration are obtained by turning off the excitation, embodied in the vector **VF**. The resulting equation possesses a non-trivial solution only if the determinant of the matrix vanishes:

$$\det[\mathbf{I}-\mathbf{VS}-\mathbf{V}(\mathbf{Q}-\mathbf{P})]=0. \tag{15}$$

A procedure, called the partition method, for solving this equation, is not easy to apply because the off-diagonal elements of the matrix are not small compared to the diagonal elements. Even at low frequency (i.e., $\mathrm{Re}(k^{[1]})R\ll1$), $B_j=B_j^{(2)}\times(k^{[1]}R)^2+O((k^{[1]}R)^2)$ for $j=\{-1,0,1\}$, so that at least three terms should be taken into account.

An iterative scheme can be employed to solve Eq. (A7) and obtain an approximate dispersion relation. This equation is re-written in the form $(1-V_lM_{ll})B_l=V_lF_l+V_l\Sigma_{m\in\mathbb{Z}}M_{lm}B_m(1-\delta_{ml})$, $\forall l\in\mathbb{Z}$. The iterative procedure for solving this linear set of equations is

$$B_l^{(0)}=\frac{V_lF_l}{1-V_lM_{ll}},$$

$$B_l^{(n)}=\frac{V_l\left(F_l+\sum_{m\in\mathbb{Z}}M_{lm}B_m^{(n-1)}(1-\delta_{ml})\right)}{1-V_lM_{ll}}, \tag{16}$$

from which it becomes apparent that the solution $B_l^{(n)}$, to any order of approximation, is expressed as a fraction, the denominator of which $\mathcal{D}_l$ (not depending on the order of approximation) can become small for certain couples (k_{1p},ω) so as to make $B_l^{(n)}$, and (possibly) the field large.

When this happens, a natural mode of the configuration, comprising the inclusions and the plate, is excited, this taking the form of a resonance with respect to $B_l^{(n)}$, i.e., with respect to a plane wave component of the field in the plate relative to the inclusions. As $B_l^{(n)}$ is related to $f_p^{[1]+}$, $f_p^{[1]-}$, T_p, and R_p, the structural resonance manifests itself for the same (k_{1p},ω) in the fields of the plate and in the air.

The approximate dispersion relation

$$\mathcal{D}_l=1-V_l\left[S_0+\sum_{p\in\mathbb{Z}}(Q_{llp}-P_{llp})\right]=0, \tag{17}$$

is the sum of a term linked to the grating embodied in $1-V_lS_0$ with a term linked to the plate embodied in $-V_l\Sigma_{p\in\mathbb{Z}}(Q_{llp}-P_{llp})$, whose expressions are give in Eq. (A4). This can be interpreted as a perturbation of the dispersion relation of the gratings by the presence of the plate.

From Eq. (A6), it is clear that if media $M^{[1]}$ and $M^{[2]}$ have properties that are close (i.e., $\rho^{[1]}\approx\rho^{[2]}$ and $c^{[1]}\approx c^{[2]}$), then the approximate dispersion relation $\mathcal{D}_l=0$ is never satisfied because $V_l\approx0$ (and so $\mathcal{D}_l\approx1$). The contrast between the medium $M^{[1]}$ and $M^{[2]}$ has to be large for the approximate dispersion relation to be satisfied. The zeroth order term of the Schlömilch series S_0 can be re-written[39] in the form $2/d\Sigma_{p\in\mathbb{Z}}1/k_{2p}^{[1]}$ (additional constants are neglected). Introducing this into Eq. (17), together with the expression of Q_{llp} and P_{llp}, gives

$$D_l = 1 - V_l \sum_{p\in\mathbb{Z}} \frac{1}{\dfrac{k_{2p}^{[1]} dD_p}{N_{lp}}} = 0, \quad \forall\, l \in \mathbb{Z}. \tag{18}$$

wherein

$$N_{lp} = 4\cos(k_{2p}^{[1]}(a+b) + 2l\theta_p)((\alpha_p^{[0]})^2 - (\alpha_p^{[1]})^2) - 4\cos(k_{2p}^{[1]}L)((\alpha_p^{[0]})^2 + (\alpha_p^{[1]})^2) + 4i\alpha_p^{[0]}\alpha_p^{[1]}\sin(k_{2p}^{[1]}L).$$

It is then convenient, for the clarity of the explanations, to consider (i) $M^{[1]}$ and $M^{[2]}$ to be non-dissipative media (i.e., medium $M^{[1]}$ and $M^{[2]}$ are perfect fluids) and (ii) the low frequency approximation of R_l (valid when $k^{[1]}R \ll 1$). The latter hypothesis ensures that the V_l reduce to $V_0 = -i\pi/4 \times (K^{[1]} - K^{[2]})/K^{[1]} = -i\pi/4 \times v_0$ and $V_{\pm 1} = -i\pi/4 \times (\rho^{[1]} - \rho^{[2]})/(\rho^{[1]} + \rho^{[2]}) = -i\pi/4 \times v_{\pm 1}$. Equation (18) then reduces to

$$D_l = 1 - \sum_{p\in\mathbb{Z}} \frac{\pi v_l}{\dfrac{4ik_{2p}^{[1]} dD_p}{N_{lp}}} = 0, \quad l = 0, \pm 1. \tag{19}$$

By referring to the work of Cutler,[17] the latter relation should be satisfied for $k_{2p}^{[1]} D_p / N_{lp}$ pure imaginary and close to zero. Because $k^{[1]} < k^{[0]}$ for the authors' application, the first condition (i.e., $k_{2p}^{[1]} D_p / N_{lp}$ pure imaginary) is obtained for $|k_{1p}| \in [k^{[0]}, k^{[1]}]$ (N_{lp} and $k_{2p}^{[1]}$ are real and D_p is pure imaginary in the non-dissipative case). The second condition (i.e., $k_{2p}^{[1]} D_p / N_{lp} = 0$) can then be satisfied only if $D_p = 0$, i.e., when $k_{1p} = k_1^\star$, or if $k_{2p}^{[1]} = 0$, i.e., when $k_{1p} = k^{[1]}$. The latter modes are Rayleigh–Wood modes of the grating (associated with the condition $k_{2p}^{[1]} = 0$) and corresponds to the bounds $|k_{1p}| = k^{[1]}$ defined by the first condition. They can also be hardly excited, especially by a normally incident plane wave. The other modes are neither modes of the plate nor Rayleigh–Wood modes of the grating but modes of the plate together with the grating of inclusions. They satisfy the relation $D_p = 0$ and correspond to evanescent waves in the ambient fluid and propagative wave in the plate. The structure of these modes is close to the one of the modes of the plate without inclusions. They are called *modified plate modes*. To each nth mode $\bar{c}_{(n)}^\star$ of the plate corresponds an infinite number of (n,p) modified plate modes $\bar{c}_{(n,p)}^\star$.

Figure 2 depicts, in the case of the rigid-frame porous (lossy) plate with inclusions, the real and imaginary parts of the solution $c_{(n,p)}^\star(\omega) = \omega / k_{(n,p)}^\star$ normalized by $c^{[0]}$ employing the mechanical characteristics of Sec. VII A, for $d = 10 \times 10^{-3}$ m. $\bar{c}_{(n,p)}^\star(\omega)$ corresponds to the intersection of $\bar{c}_n^\star(\omega)$ as depicted in Sec. IV with $\bar{c}_p(\omega) = \omega/(k_{1p} c^{[0]})$. k_{1p} being real, the associated attenuation corresponds to $\mathrm{Im}(\bar{c}_n^\star(\omega))$ at the frequency $\bar{c}_n^\star(\omega)$ and $\mathrm{Re}(\bar{c}_p(\omega))$ intersect. The modified plate mode can now be excited by an incident plane (bulk) wave, because of the summation over the index p, which allows the existence of evanescent waves in $\Omega_{[0\pm]}$. When a modified plate mode is excited, the structure of the associated waves allow the entrapment of a part of the energy inside the plate and thus to an increase in the absorption.

VI. EVALUATION OF THE REFLECTION, TRANSMISSION, AND ABSORPTION COEFFICIENTS

The developed form of the conservation of energy relation is

$$1 = \mathcal{A} + \mathcal{R} + \mathcal{T}, \tag{20}$$

where $\mathcal{A}$, $\mathcal{R}$, and $\mathcal{T}$ are the absorption, hemispherical reflection, and hemispherical transmission coefficients, respectively. The latter two coefficients are defined by

$$\mathcal{R} = \sum_{p\in\mathbb{Z}} \frac{\mathrm{Re}(k_{2p}^{[0]})\|R_p(\omega)\|^2}{k_2^{[0]i}\|A^i\|^2} = \sum_{p=\bar{p}^-}^{\bar{p}^+} \frac{k_{2p}^{[0]}\|R_p(\omega)\|^2}{k_2^{[0]i}\|A^i\|^2},$$

$$\mathcal{T} = \sum_{p\in\mathbb{Z}} \frac{\mathrm{Re}(k_{2p}^{[0]})\|T_p(\omega)\|^2}{k_2^{[0]i}\|A^i\|} = \sum_{p=\bar{p}^-}^{\bar{p}^+} \frac{k_{2p}^{[0]}\|T_p(\omega)\|^2}{k_2^{[0]i}\|A^i\|}, \tag{21}$$

wherein $\bar{p}$ is such that $(k_1^i + 2\pi(\bar{p} \pm \mp 1)/d)^2 > (k^{[0]})^2 \geq (k_1^i + 2\pi\bar{p}^{\pm}/d)^2$ and the expressions of R_p and T_p are given in Eq. (12), while $\mathcal{A}$ involves non-vanishing surface integrals on Γ_a, Γ_b, and Γ because of viscous effects. Because of the previous argument and because of the complicated shape of $\Omega_{[1]}$ over which some integration should be carried on for the evaluation of the absorption of the porous material itself, $\mathcal{A}$ will be calculated by $\mathcal{A} = 1 - \mathcal{R} - \mathcal{T}$.

VII. NUMERICAL RESULTS AND DISCUSSION

The ambient and saturating fluids are air ($\rho^{[0]} = \rho_f = 1.213$ kg m^{-3}, $c^{[0]} = \sqrt{\gamma P_0/\rho_0}$, with $P_0 = 1.01325 \times 10^5$ Pa and $\gamma = 1.4$, $\eta = 1.839 \times 10^{-5}$ kg m^{-1} s^{-1}). The inclusions are either occupied by melamine-foam (which defines the so-called type 1 sample) or with an acoustically-hard material (for which a Neumann condition prevails on Γ and which defines the so-called type 2 sample). The latter condition is easily encountered for acoustic waves that propagate in rigid-frame porous plate containing inclusions made out of a material whose characteristic impedance is very large compared to that of the porous medium, the latter being very close to the characteristic impedance of the air medium; any elastic materials, such as metals or acrylic plastics, are suitable. Furthermore, the domain Ω_2 does not have to be completely filled with such a material in order for the Neumann boundary condition to prevail; elastic tubes are an example of such inclusions. In practice, this enables the configuration to be lightweight.

The medium $M^{[1]}$ is characterized by $\phi = 0.96$, $\alpha_\infty = 1.07$, $\Lambda = 273 \times 10^{-6}$ m, $\Lambda' = 672 \times 10^{-6}$ m, and $\sigma = 2843$ N s m^{-4}, while the melamine-foam is characterized by $\phi = 0.99$, $\alpha_\infty = 1.001$, $\Lambda = 150 \times 10^{-6}$ m, $\Lambda' = 250 \times 10^{-6}$ m, and $\sigma = 12 \times 10^3$ N s m^{-4}. Melamine foam is more absorptive than the polyurethane foam that occupies the plate, but, on the whole, their mechanical characteristics are rather close. The incident angle is $\theta^i = \pi/2$.

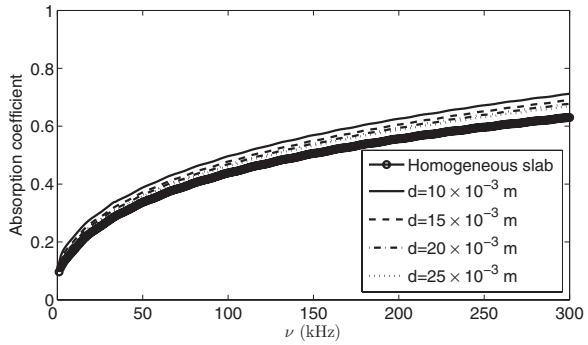

FIG. 3. Absorption coefficients for various center-to center distances and for type 1 samples.

A. Numerical results for an ultrasonic wave incident on a rigid-frame porous plate with a periodic distribution of inclusions

First, an infinite layer 1×10^{-2} m thick and filled with a polymer foam $M^{[1]}$ is considered. Figure 3 depicts the absorption coefficients for type 1, while Fig. 4 depicts the hemispherical reflection, hemispherical transmission, and absorption coefficients for type 2 samples when the radius of the inclusions is equal to $R=2.5\times10^{-3}$ m and the center-to-center distance between inclusion varies from $d=1\times10^{-2}$ m to $d=2.5\times10^{-2}$ m.

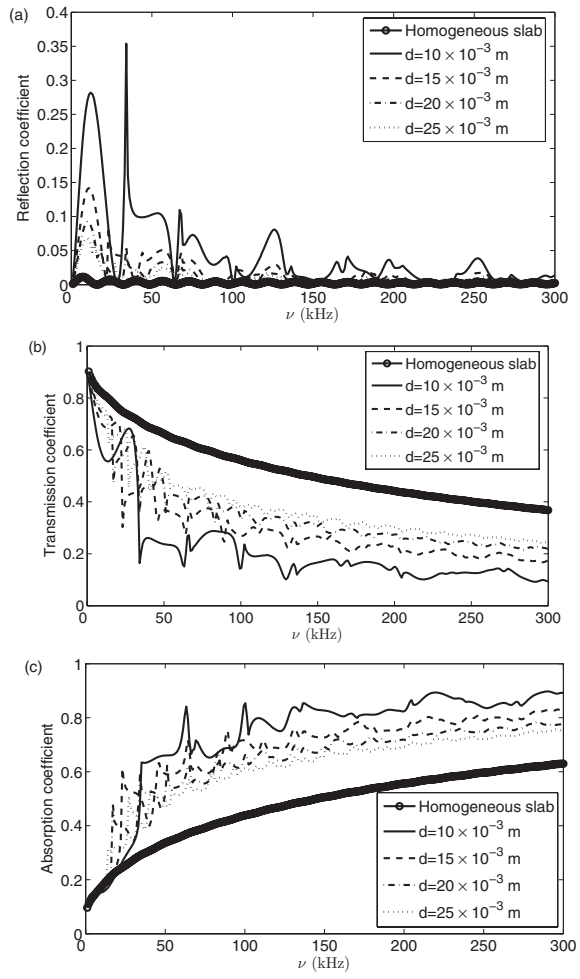

FIG. 4. Hemispherical transmission coefficients (a), hemispherical reflection coefficients (b), and absorption coefficients (c) for various center-to-center distances and for type 2 samples.

For weak contrast type inclusions, no substantial modifications of the hemispherical reflection, transmission, and absorption are noticed. As shown in Sec. VI, when a periodic set of weak contrast inclusions is added to the plate, the dispersion relation cannot vanish so that no modes of the configuration can be excited. The absorption coefficient increases slowly when d decreases while the transmission decreases. The reflection coefficient is practically unmodified by the addition of the periodic set of inclusions. The small increase in the absorption coefficient is due to the fact that a dissipative plate is partially filled with a more dissipative medium, the acoustical properties of the whole configuration being modified in proportion to the ratio of the volume of $M^{[2]}$ to that of $M^{[1]}$.

The results are completely different for large contrast type 2 inclusions for which substantial modifications of the hemispherical reflection, transmission, and absorption are encountered. For frequencies higher than a frequency offset, which depends on the center-to-center distance between inclusions, the hemispherical transmission coefficient decreases substantially, this being associated with an increase in the absorption coefficient. On the contrary, the hemispherical reflection coefficient increases, but less than the decrease in the hemispherical transmission coefficient. The latter seems to be mainly due to the first reflection (in terms of the time domain reflection) on the inclusion when propagative waves are preponderant in the system. Both the hemispherical reflection and transmission coefficient spectra exhibit minima at the same frequencies, at which the absorption coefficient is maximal.

The frequency offset and the maxima of the absorption coefficient (corresponding to minima of the hemispherical reflection and transmission) are linked to, and explained by, the excitation of the modified plate mode. The frequency offset corresponds to the excitation of the first modified plate mode of the configuration. This frequency is also dependent on the thickness of the plate, on the mechanical characteristics of the material that fills the plate, and on the periodicity of the grating. The larger the d is, the smaller the frequency offset is. Below this frequency, no particular modification of the absorption is noticed because waves in the ambient fluid are mainly propagative. Beyond this frequency, evanescent waves in the ambient fluid, associated with modified plate mode excitation, are involved and cause an entrapment of the energy inside the plate, this leading to an increase in the absorption coefficient. This is particularly noticeable for the maxima of the absorption (minima of the hemispherical reflection and transmission) coefficients that are located at the higher modified plate mode natural frequencies. For these frequencies, evanescent waves in the ambient fluid are preponderant and cause an important entrapment of the energy inside the plate.

For a fixed frequency beyond the offset, the increase in the absorption coefficient is dependent (Fig. 3) on the period of the gratings with fixed inclusion radius (large for a small period and small for a large period) and dependent (Fig. 5)

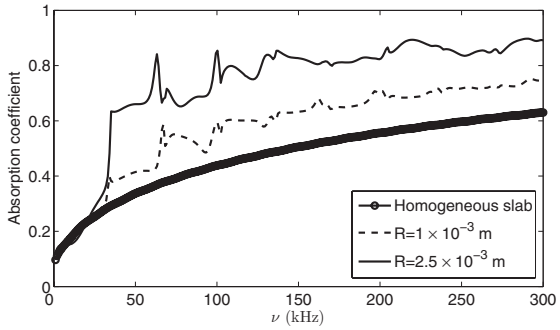

FIG. 5. Comparison of the absorption coefficient for $R=2.5\times10^{-3}$ m and $R=1\times10^{-3}$ m. Type 2 inclusions with $d=10\times10^{-3}$ m.

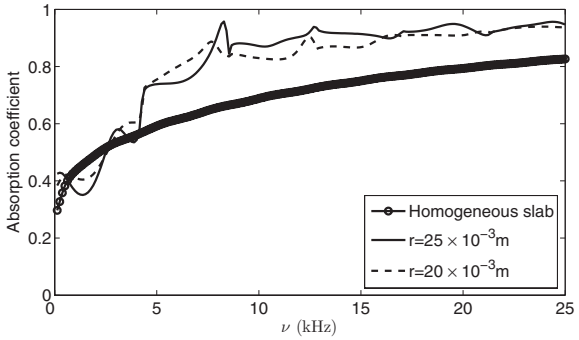

FIG. 7. Absorption coefficients for $R=25\times10^{-3}$ m and $R=20\times10^{-3}$ m. Type 2 inclusions with $d=80\times10^{-3}$ m.

on the radius of the gratings for a fixed period (large for a large radius and small for a small radius). This means that the sought-for increase in the absorption is strongly linked to the determination of the configuration that allows an optimal excitation of modified plate modes. Increasing the period for fixed radius inclusions, or decreasing the radius of the inclusion for a fixed period, both reduce the impact of the inclusions on the global response of the configuration and thus lessen the possibility of modified plate mode excitation. The increase in the absorption coefficient appears to follow the ratio radius over period (r/d).

B. Use of periodic set of high-contrast inclusions for the absorption of audible sound

From the results of Sec. VII A, it can be inferred (i) that the addition of a periodic set of high-contrast inclusions to a rigid-frame porous plate induces an increase in the absorption of the latter for frequencies that are equal or higher than the natural frequency of the first modified plate mode of the configuration and (ii) that the increase in the absorption is all the greater the larger is r/d. The audible frequency range extends from 15–20 Hz to 16–23 kHz. The natural frequency of the first modified plate mode is attained approximately for $\bar{c}_{(1,1)}=(\omega_{(1,1)}d)/(2\pi c^{[0]})\approx0.95$ for normal incident plane waves. The frequency offset is proportional to $1/d$. The lower is the frequency offset, i.e., the lower the resonance frequency of the first modified plate mode, the larger must be the distance that separates adjacent inclusions. The configuration (thickness of the plate, periodicity, and radius) will also be larger for the absorption of audible sound than it is for ultrasound. For example, to increase the absorption coefficient for frequencies that are higher than 4000 Hz, d must be chosen such that $d\approx0.95c^{[0]}/\nu_{(1,1)}\approx81.2\times10^{-3}$ m. $d=80\times10^{-3}$ m is considered hereafter. When compared to the periodicity used in Sec. VII A, d is multiplied by a factor of 8. Two cases are also considered hereafter: $R=25\times10^{-3}$ m and $R=20\times10^{-3}$ m. In practice, the design of acoustical absorbing materials is submitted to constraints in terms of weight and size. The thickness of the plate is thus chosen to be $L=60\times10^{-3}$ m, which corresponds to a radius over the plate thickness ratio $(R/L=25/60\approx0.41)$ larger than for the ultrasonic case $(R/L=2.5/10\approx0.25)$.

Figure 6 depicts the real and imaginary parts of the roots of the dispersion relation in the case of a $L=60\times10^{-3}$ m thick plate filled with $M^{[1]}$ material. The modified plate mode frequencies and associated attenuation are pinpointed in this figure when $d=80\times10^{-3}$ m. The frequency of the first modified plate mode is found to occur at $\nu_{(1,1)}\approx4100$ Hz. Figure 7 depicts the absorption coefficients for type 2 inclusions of radius $R=25\times10^{-3}$ m and $R=20\times10^{-3}$ m. The absorption is larger in case of the larger radius for frequencies higher than $\nu_{(1,1)}\approx4100k$ Hz. The hemispherical reflection and transmission coefficients present minima associated with maxima of the absorption coefficient at the resonance frequencies of the modified plate modes of higher order. The mechanism by the which the absorption is increased is the one described in Sec. VII A (relative to ultrasonic solicitation).

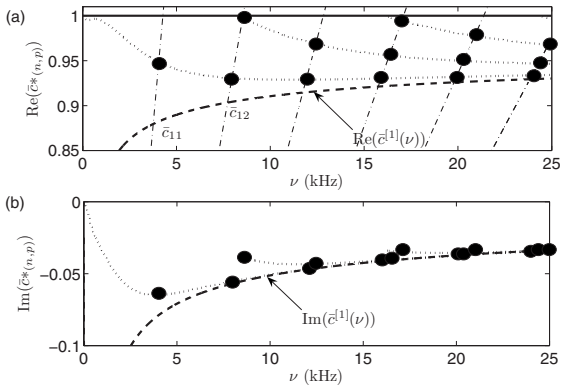

FIG. 6. (a) Modified plate mode and (b) its associated attenuation for a period $d=80\times10^{-3}$ m. The modified plate mode and associated attenuation locations are indicated by dots.

VIII. CONCLUSION

It is shown that high-contrast, periodically-arranged, macroscopic inclusions in a porous plate induce an increase in the absorption coefficient, mainly associated with a decrease in the hemispherical transmission coefficient for frequencies that are higher than a frequency offset. This effect is due to the excitation of the modified plate modes. Expressed differently, the excitation of something similar to a plate mode of the initial macroscopically-homogeneous plate is enabled by the presence of the periodic set of inclusions. The frequency offset of substantial modification of response (with respect to that of the macroscopically-homogeneous plate) corresponds to the frequency of the first modified plate mode of the configuration, while large absorption peaks are

also encountered at the resonance frequencies of the higher order modified plate modes. The type of waves (evanescent in the half spaces above and below the plate, propagative within the plate) associated with these modified plate modes helps to understand why the periodic set of inclusions is necessary for modal excitation and why energy is trapped in the plate at resonance.

The natural frequencies of the modified plate modes were evaluated by referring to the Cutler-modes of gratings through an approximate dispersion relation.

The reflection coefficients were found to be of the same order as those in the absence of inclusions for low-contrast inclusions and to be higher than those in the absence of inclusions for high-contrast inclusions.

Further work should deal with the reduction in the hemispherical reflection coefficient. A possible manner for reducing the latter is by acting on the surface geometry of the plate. A first approach could consist in the addition of a homogenized layer of double porosity.[10]

APPENDIX A: DETERMINATION OF THE UNKNOWNS

1. Application of the continuity conditions across the interfaces Γ_a and Γ_b

Applying successively $\int_{-d/2}^{d/2} \cdot dx_1$ to the continuity of the pressure field and of the normal component of the velocity across Γ_a and Γ_b, Eq. (4), and making use of the orthogonality relation $\int_{-d/2}^{d/2} e^{i(k_{1n}-k_{1l})x_1} dx_1 = d\delta_{nl}$, $\forall (l,n) \in \mathbb{Z}^2$, gives rise to the system of linear equations

$$A^i \delta_{p0} + R_p - f_p^{[1]-} e^{-ik_{2p}^{[1]}a} - f_p^{[1]+} e^{ik_{2p}^{[1]}a} - \sum_{l\in\mathbb{Z}} B_l K_{pl}^{+} e^{ik_{2p}^{[1]}a} = 0, \tag{A1a}$$

$$-A^i \alpha_p^{[0]} \delta_{p0} + R_p \alpha_p^{[0]} + f_p^{[1]-} \alpha_p^{[1]} e^{-ik_{2p}^{[1]}a} - f_p^{[1]+} \alpha_p^{[1]} e^{ik_{2p}^{[1]}a} - \sum_{l\in\mathbb{Z}} B_l K_{pl}^{+} \alpha_p^{[1]} e^{ik_{2p}^{[1]}a} = 0, \tag{A1b}$$

$$T_p - f_p^{[1]-} e^{-ik_{2p}^{[1]}b} - f_p^{[1]+} e^{ik_{2p}^{[1]}b} - \sum_{l\in\mathbb{Z}} B_l K_{pl}^{-} e^{-ik_{2p}^{[1]}b} = 0. \tag{A1c}$$

$$-T_p \alpha_p^{[0]} + f_p^{[1]-} \alpha_p^{[1]} e^{-ik_{2p}^{[1]}b} - f_p^{[1]+} \alpha_p^{[1]} e^{ik_{2p}^{[1]}b} + \sum_{l\in\mathbb{Z}} B_l K_{pl}^{-} \alpha_p^{[1]} e^{-ik_{2p}^{[1]}b} = 0, \tag{A1d}$$

for the resolution of R_p, T_p, and $f^{[1^{\pm}]}$ in terms of B_m, $\forall m \in \mathbb{Z}$ and wherein $\alpha_p^{[i]} = k_{2p}^{[i]}/\rho^{[i]}$ and $i = 0^{\pm}, 1$.

2. Application of the multipole method

Introducing the expressions of $f_p^{[1]-}$ and $f_p^{[1]+}$ in terms of B_l obtained from Eq. (A1) into Eq. (11) leads to an expression of $\tilde{p}^{[1^{\pm}]}(\mathbf{x})$ in the Cartesian coordinate system in terms of B_l, $\forall l \in \mathbb{Z}$. Central to the multipole method are the local field expansion or multipole expansions around each inclusion.[13–15] Because $p(\mathbf{r})$ satisfy a Helmholtz equation inside and outside the cylinder of the unit cell, in the vicinity of the latter (i.e., $\forall \mathbf{r} \le d-R$), $\tilde{p}^{[1]}(\mathbf{r})$ can be written in the form

$$\tilde{p}^{[1]}(\mathbf{r}) = \sum_{l\in\mathbb{Z}} (B_l H_l^{(1)}(k^{[1]}r) + A_l J_l(k^{[1]}r)) e^{il\theta}, \tag{A2}$$

wherein A_l are the coefficients of the locally incident field to the central cylinder, $H_l^{(1)}$ is the lth Hankel function of first kind, and J_l is the lth bessel function. To proceed further, the Cartesian form must be converted to the cylindrical harmonic form by means of $x_1 = r\cos(\theta)$, $x_2 = r\sin(\theta)$, $k_{1p} = k^{[1]}\cos(\theta_p)$, and $k_{2p}^{[1]} = k^{[1]}\sin(\theta_p)$, together with the identity $e^{ikr\cos(\theta-\theta_p)} = \sum_{m\in\mathbb{Z}} i^m J_m(kr) e^{im(\theta-\theta_p)}$:

$$\tilde{p}^{[1]}(\mathbf{r}) = \sum_{l\in\mathbb{Z}} \left[B_l H_l^{(1)}(k^{[1]}r) + \left(\sum_{m\in\mathbb{Z}} M_{lm} B_m + F_l \right) J_l(k^{[1]}r) \right] e^{il\theta}, \tag{A3}$$

with $M_{lm} = S_{l-m} + \sum_{p\in\mathbb{Z}} (Q_{lmp} - P_{lmp})$, $F_l = \sum_{p\in\mathbb{Z}} (J_{lp}^{-} F_p^{[1]-} + J_{lp}^{+} F_p^{[1]+})$, $J_{lp}^{\pm} = i^l e^{\mp il\theta_p}$, and wherein

$$F_p^{[1]\pm} = \left[\pm 2\alpha_p^{[0]} \frac{\alpha_p^{[0]} \mp \alpha_p^{[1]}}{D_p} \right] e^{\mp ik_{2p}^{[1]}b} \delta_{p0} A^i,$$

$$Q_{\mathrm{lmp}} = 4(-i)^{m-l} \frac{(\alpha_p^{[0]})^2 - (\alpha_p^{[1]})^2}{dk_{2p}^{[1]} D_p} \times \cos(k_{2p}^{[1]}(a+b) + (l+m)\theta_p),$$

$$P_{\ln p} = 4(-i)^{m-l} e^{ik_{2p}^{[1]}L} \frac{(\alpha_p^{[0]} - \alpha_p^{[1]})^2}{dk_{2p}^{[1]} D_p} \cos((m-l)\theta_p),$$

$$S_l = \sum_{j=1}^{\infty} H_l^{(1)}(k^{[1]}jd)[e^{ik_1^i jd} + (-1)^l e^{-ik_1^i jd}]. \tag{A4}$$

S_l is the Schlömilch series often referred to as a lattice sum, and D_p as defined Eq. (13).

Identifying Eq. (A2) with Eq. (A3), it follows that

$$A_l = \sum_{m\in\mathbb{Z}} M_{lm} B_m + F_l. \tag{A5}$$

At this point, the two equations (5) and (6) are accounted-for. It is well-known that the coefficients of the scattered field B_l and those of the locally incident field A_l are linked by a matrix relation [derived form the continuity conditions Eqs. (5)] depending on the parameters of the cylinder only $B_l = V_l A_l$, with

$$V_l = \frac{\gamma^{[1]} \dot{J}_l(\chi^{[1]}) J_l(\chi^{[2]}) - \gamma^{[2]} \dot{J}_l(\chi^{[2]}) J_l(\chi^{[1]})}{\gamma^{[2]} \dot{J}_l(\chi^{[2]}) H_l^{(1)}(\chi^{[1]}) - \gamma^{[1]} \dot{H}_l^{(1)}(\chi^{[1]}) J_l(\chi^{[2]})}, \tag{A6}$$

wherein $\gamma^{[j]} = k^{[j]}/\rho^{[j]}$, $\chi^{[j]} = k^{[j]}R$, $j = 0, 1$, and $\dot{Z}_l(x) = dZ_l(x)/dx$. Denoting by $\mathbf{B}$ the infinite column matrix of components B_l, Eq. (A5) together with Eq. (A6) may be written in the matrix form

$$(\mathbf{I} - \mathbf{VM})\mathbf{B} = (\mathbf{I} - \mathbf{VS} - \mathbf{V}(\mathbf{Q} - \mathbf{P}))\mathbf{B} = \mathbf{VF}, \tag{A7}$$

with $\mathbf{F}$ the column matrix of lth element F_l, $\mathbf{I}$ the identity matrix, $\mathbf{V}$ the diagonal matrix of component V_l, and $\mathbf{S}$, $\mathbf{Q}$, and $\mathbf{P}$ three square matrices whose (l,m)th elements are S_{l-m}, $\Sigma_{p\in\mathbb{Z}} Q_{lmp}$, and $\Sigma_{p\in\mathbb{Z}} P_{lmp}$, respectively.

Remark. In the case of a Neumann type boundary condition equation (5), expression Eq. (A6) takes the form $V_l^{\mathcal{N}} = -\dot{J}_l(k^{[1]}R)/\dot{H}_l^{(1)}(k^{[1]}R)$.

APPENDIX B: NUMERICAL RECIPES

The infinite sum $\Sigma_{m\in\mathbb{Z}}$ over the indices of the modal representation of the diffracted field by a cylinder is truncated as $\Sigma_{m=-M}^{M}$ such that[40] $M=\text{int}(\text{Re}(4.05\times(k^{[1]}R)^{1/3}+k^{[1]}R))+10$.

On the other hand, the infinite sum $\Sigma_{p\in\mathbb{Z}}$ over the indices of the k_{1p} is found to depend on the frequency and on the period of the grating. An empirical rule is employed, determined by performing a large number of numerical experiments $\Sigma_{p=-P}^{P}$ such that $P=\text{int}(d/2\pi(3\ \text{Re}(k^{[1]})-k_1^i))+5$. In the latter equations, int(a) represents the integer part of a. Considering the foam plate without dissipation, $k_2^{[1]}$ is the last vertical wave number to become purely imaginary when $|p|$ increases. The previous numerical rule also ensures that $k_{2p}^{[1]}=i\sqrt{2}\|k^{[1]}\|$ (nondissipative case) with an added security term equal 5.

Finally, the infinite sum embedded in S_{m-l} in Eq. (A2) (lattice sum) $\Sigma_{j=1}^{\infty}$ is found to be slowly convergent, particularly in the absence of dissipation, and is found to be strongly dependent on the indices $m-l$. A large literature exists on this problem.[41,42] Here, the fact that the medium $M^{[1]}$ is dissipative greatly simplifies the evaluation of the Schlömilch series. The superscript J in S_{m-l}^{J} identifies the integer over which the sum is performed, i.e., $\Sigma_{j=1}^{J}$. This sum is carried out until the conditions $|\text{Re}((S_{m-l}^{J+1}-S_{m-l}^{J})/S_{m-l}^{J})|\leq 10^{-5}$ and $|\text{Im}((S_{m-l}^{J+1}-S_{m-l}^{J})/S_{m-l}^{J})|\leq 10^{-5}$ are reached.

[1] L. Brekovskikh, *Waves in Layered Media* (Academic, New York, 1960).
[2] U. Ingard, *Notes on Sound Absorption Technology* (Noise Control Foundation, Poughkeepsie, 1994).
[3] O. Tanneau, J. Casimir, and P. Lamary, "Optimization of multilayered panels with poroelastic components for an acoustical transmission objective," J. Acoust. Soc. Am. **120**, 1227–1238 (2006).
[4] M. Biot, "Theory of propagation of elastic waves in fluid-saturated porous solid," J. Acoust. Soc. Am. **28**, 168–178 (1956).
[5] M. Biot, "Mechanics of deformation and acoustic propagation in porous media," J. Appl. Phys. **33**, 1482–1498 (1962).
[6] D. Johnson, J. Koplik, and R. Dashen, "Theory of dynamic permeability and tortuosity in fluid-saturated porous media," J. Fluid Mech. **176**, 379–402 (1987).
[7] K. Attenborough, "Acoustical characteristics of porous materials," Phys. Rep. **82**, 179–227 (1982).
[8] J.-F. Allard, *Propagation of Sound in Porous Media: Modelling Sound Absorbing Materials* (Chapman & Hall, London, 1993).
[9] L. De Ryck, J.-P. Groby, P. Leclaire, W. Lauriks, A. Wirgin, C. Depollier, and Z. Fellah, "Acoustic wave propagation in a macroscopically inhomogeneous porous medium saturated by a fluid," Appl. Phys. Lett. **90**, 181901 (2007).
[10] X. Olny and C. Boutin, "Acoustic wave propagation in double porosity media," J. Acoust. Soc. Am. **114**, 73–89 (2003).
[11] C. Boutin, P. Royer, and J.-L. Auriault, "Acoustic absorption of porous surfacing with dual porosity," Int. J. Solids Struct. **35**, 4709–4737 (1998).
[12] V. Tournat, V. Pagneux, D. Lafarge, and L. Jaouen, "Multiple scattering of acoustic waves and porous absorbing media," Phys. Rev. E **70**, 026609 (2004).
[13] L. Botten, N. Nicorovici, A. Asatryan, R. McPhedran, C. Poulton, C. de Sterke, and P. Robinson, "Formulation for electromagnetic scattering and propagation through grating stacks of metallic and dielectric cylinders for photonic crystal calculations. Parti method," J. Opt. Soc. Am. A Opt. Image Sci. Vis **17**, 2165–2176 (2005).
[14] D. Felbacq, G. Tayeb, and D. Maystre, "Scattering by a random set of parallel cylinders," J. Opt. Soc. Am. A Opt. Image Sci. Vis **11**, 2526–2538 (1994).
[15] S. Wilcox, L. Botten, R. McPhedran, C. Poulton, and C. de Sterke, "Modeling of defect modes in photonic crystals using the fictitious source superposition method," Phys. Rev. E **71**, 056606 (2005).
[16] R. Wood, "A suspected case of the electrical resonance of minute metal particles for light-waves. A new type of absorption," Proc. Phys. Soc. London **18**,166–182 (1902).
[17] C. Cutler, "Electromagnetic waves guided by corrugated structures," Technical Report No. MM 44-160-218, Bell Telephone Laboratories, 1944.
[18] B. Budiansky, "On the elastic moduli of some heterogeneous materials," J. Mech. Phys. Solids **13**, 223–227 (1965).
[19] Z. Hashin and S. Shtrikman, "A variational approach to the theory of the elastic behaviour of multiphase materials," J. Mech. Phys. Solids **11**, 127–140 (1963).
[20] T. Wu, "The effect of inclusion shape on the elastic moduli of the two-phase material," Int. J. Solids Struct. **1**, 1–8 (1966).
[21] J. Cuomo, J. Ziegler, and J. Woodhall, "A new concept for solar energy thermal conversion," Appl. Phys. Lett. **26**, 557–559 (1975).
[22] C. Horwitz, "Solar-selective globular metal films," J. Opt. Soc. Am. **68**, 1032–1038 (1978).
[23] J. Joannopoulos, R. Meade, and J. Winn, *Photonic Crystals; Molding the Flow of Light* (Princeton University Press, Princeton, 1995).
[24] E. Yablonovitch, "Photonic band-gap structures," J. Opt. Soc. Am. B **10**, 283–295 (1993).
[25] V. Veselago, "The electrodynamics of substances with simultaneous negative value of e and m," Sov. Phys. Usp. **10**, 509–514 (1968).
[26] P.-Y. Bard and A. Wirgin, "Effects of buildings on the duration and amplitude of ground motion in Mexico City," Bull. Seismol. Soc. Am. **86**, 914–920 (1996).
[27] J.-P. Groby and A. Wirgin, "Seismic motion in urban sites consisting of blocks in welded contact with a soft layer overlying a hard half space," Geophys. J. Int. **172**, 725–758 (2008).
[28] A. Khelif, B. Djafari-Rouhani, V. Laude, and M. Solal, "Coupling characteristics of localized phonons in photonic crystal fibers," J. Appl. Phys. **94**, 7944–7946 (2003).
[29] V. Laude, M. Wilm, S. Benchabane, and A. Khelif, "Full band gap for surface acoustic waves in a piezoelectric phononic crystal," Phys. Rev. E **71**, 036607 (2005).
[30] M. Wilm, K. Khelif, S. Ballandras, V. Laude, and B. Djafari-Rouhani, "Out-of-plane propagation of elastic waves in two-dimensional phononic band-gap material," Phys. Rev. E **67**, 065602 (2003).
[31] A. de Bruijn, "Anomalous effects in the sound absorption of periodically uneven surfaces," Acustica **24**, 75–84 (1971).
[32] L. Kelders, J.-F. Allard, and W. Lauriks, "Ultrasonic surface waves above rectangular-groove gratings," J. Acoust. Soc. Am. **103**, 2730–2733 (1998).
[33] B. Sapoval, B. Hebert, and S. Russ, "Experimental study of a fractal acoustical cavity," J. Acoust. Soc. Am. **105**, 2014–2019 (1999).
[34] J.-P. Groby, E. Ogam, and A. Wirgin, "Acoustic response of a periodic distribution of macrosocopic inclusions within a rigid frame porous plate," Waves Random Complex Media **18**, 409–433 (2008).
[35] J.-F. Allard and Y. Champoux, "New empirical equations for sound propagation in rigid frame porous materials," J. Acoust. Soc. Am. **91**, 3346–3353 (1992).
[36] J.-P. Groby, L. De Ryck, P. Leclaire, A. Wirgin, W. Lauriks, R. P. Gilbert, and Y. Xu, "Use of specific Green's functions for solving direct problems involving a heterogeneous rigid frame porous medium slab solicited by the acoustic waves," Math. Methods Appl. Sci. **30**, 91–122 (2007).
[37] J.-P. Groby and C. Tsogka, "A time domain method for modeling viscoacoustic wave propagation," J. Comput. Acoust. **14**, 201–236 (2006).
[38] J.-P. Groby and A. Wirgin, "2D ground motion at a soft viscoelastic layer/hard substratum site in response to SH cylindrical waves radiated by deep and shallow line sources: Numerical results," Geophys. J. Int. **163**, 192–224 (2005).
[39] C. Linton and I. Thompson, "Resonant effects in scattering by periodic arrays," Wave Motion **44**, 165–175 (2007).
[40] P. Barber and S. Hill, *Light Scattering by Particles: Computation Methods*, Advanced Series in Applied Physics 2 (World Scientific, London, 1990), Chaps. 2 and 30.
[41] V. Twersky, "On scattering of waves by the infinite grating of circular cylinders," IRE Trans. Antennas Propag. **10**, 737–765 (1962).
[42] C. Linton, "Schlömilch series that arise in diffraction theory and their efficient computation," J. Phys. A **39**, 3325–3339 (2006).